Localization of Coated Iron Oxide (Fe_3O_4) Nanoparticles on Tomato Seeds and their Effects on Growth

Elizabeth C. H. T. Lau[1], Lucas B. Carvalho[2], Anderson E. S. Pereira[2], Gabriel S. Montanha[3], Camila G. Corrêa[3], Hudson W. P. Carvalho[3], Alexey Y. Ganin[4], Leonardo F. Fraceto[2*], Humphrey H. P. Yiu[1*]

[1] Chemical Engineering, School of Engineering and Physical Sciences, Heriot-Watt University, Edinburgh, EH14 4AS, U.K.

[2] São Paulo State University (UNESP), Institute of Science and Technology, Avenida Três de Março 511, CEP 18087-180, Sorocaba, SP, Brazil

[3] University of São Paulo, Center for Nuclear Energy in Agriculture, Piracicaba, SP, 13416000, Brazil

[4] School of Chemical, University of Glasgow, Joseph Black Building, University Avenue, Glasgow, G12 8QQ, U.K.

*Corresponding authors: Humphrey H. P. Yiu (H.H.Yiu@hw.ac.uk) and Leonardo F. Fraceto (leonardo.fraceto@unesp.br)

Abstract

Food demand due to the growing population globally has been stretching the agriculture sector to the limit. This demands the cultivation of plants in shrinking land areas which makes the search for highly effective systems for plant nutrition and pest control important. In this context, the application of nanoparticles (NPs) in agriculture can have a transformative effect on food production techniques as it can enable the delivery of bioactive agents (including growth factors, pesticides and fungicides) directly to plants. Herein we report the application of unfunctionalized as well as amine-functionalized and polycaprolactone-coated Fe_3O_4 nanoparticles to seed treatment in tomato (*Solanum Lycopersicum*). The study reveals that the treatment has no side effects on plant germination and development. Furthermore, the translocation of NPs in seeds and seedlings post-treatment depends on the surface functionalization of the NPs. XRF analysis of seedlings suggested that around 66% of unfunctionalized Fe_3O_4 nanoparticles were translocated in the cotyledons while only 50% of functionalized NPs (both amine and PCL). Our results demonstrate that all particles were uptaken by the seeds, thus suggesting that the functionalized NPs can act as a versatile platform for delivering of active compounds, such as fungicides and growth factor agents.

Keywords: Magnetite, polycaprolactone, APTES, silanization, delivery, seedling, agriculture, μ-XRF.

1. Introduction

Metallic and metal oxide nanoparticles show a significant potential to provide eco-friendly solutions for improving agricultural productivity.[1] They had been used for pest control, enhancing plant nutrition, as well as improving crop production. There have been several studies on the effect of nanoparticles to a plant system, but the mechanism of interactions between nanoparticles and plant cells is still poorly understood.[2]

There are two pathways for nanoparticles to be taken up by plants. In the symplastic pathway, translocations depend mainly on the movement of water and substances between the cytoplasm of adjacent cells by specific structures called plasmodesmata. In the apoplastic pathway, the translocation of nanoparticles is outside the cells, through the extracellular cavity.[3] However, nanoparticle access to the plant cell will depend on its size, morphology, crystal structure, coating type, surface charge, and hydrophobicity.[4,5] Studies have shown that the design of nanoparticles can alter the mechanism of plant growth at an early stage, causing functional damage associated with tissue differentiation and solute transport.[6]

Studies on the effects of metallic and metal oxide nanoparticles on the plants development, the physiological and biochemical processes in plants can be found in the literature.[7] Among these studies, new strategies have been successful in modulating the uptake pathway by plants, as well as the translocation.[8] For example, polyvinylpyrrolidone (PVP) polymer coated gold nanoparticles have been shown to enhance leaf surface uptake of nanoparticles, alter aggregation potential and cellular effects.[8] Moreover, positively charged gold nanoparticles coated with polyethyleneimine (PEI) induced mucilage production, which entrapped the particles and reduced their uptake in Arabidopsis thaliana plants.[9] On the other hand, negatively-charged citrate coated gold nanoparticle were taken up and translocated in the roots. Kumar et al. (2013) [10] showed that gold nanoparticles coated with biomolecules extracted from seeds of *Syzygium cumini L.* increased the seed germination by 10-15% and seedling size by about 1.5 times. Also, after the plant development, an increase in the antioxidant enzymes activity (by 1.24-2.83 times) was observed.[10] In addition, the enhanced germination ratio could also be caused by the biomolecules from vegetal extract other than by the gold nanoparticles.

Iron oxide nanoparticles have already shown some positive effects on plant growth. For example, iron oxide nanoparticles was shown to be able to regulate the level of phytohormones and antioxidant enzymes in peanuts plants (*Arachis hypogaea*), in turn to promote a better plant development.[11] Rui et al. (2016)[11] showed that iron oxide (γ-Fe_2O_3) nanoparticles had the potential to act as a fertilizer. A study on *Arachis hypogaea* showed that these Fe_2O_3 nanoparticles promoted an increase in the plant's biomass, their photosynthetic activity and the uptake of the Fe^{3+} ions by plants. Hussain et al. (2019) 12 used iron oxide (Fe_3O_4) nanoparticles as an alternative for soil remediation when they germinated Triticum aestivum seeds in soils contaminated with cadmium. After 125 days, the absorption of cadmium by plant was reduced by 53% and the phytotoxic effects were alleviated. Moreover, several studies have reported that iron oxide nanoparticles can increase seed germination,[13] seedling vigor, plant biomass, and yield, and also enhance physiological function.[11–15] However, in our best knowledge, there is no study found in the literature on the effect of the surface coating of iron oxide nanoparticles on plant growth.

In this work, we report the synthesis and characterization of amine-functionalized, using 3-aminopropyltriethoxysilane (APTES), and polycaprolactone-coated iron oxide (Fe_3O_4) magnetic nanoparticles (MNP). The NPs were evaluated in terms of their phytotoxicity and their uptake by plants was studied in detail, in order to demonstrate their potential as carrier systems for agricultural application.

2. Materials and methods

2.1 Materials

Iron (III) chloride hexahydrate ($FeCl_3 \cdot 6H_2O$, ACS Reagent) and polycaprolactone (PCL, Mw~14000 Da) were supplied by Sigma Aldrich, while iron (II) chloride tetrahydrate ($FeCl_2 \cdot 4H_2O$, 99%) was purchased from Acros Organics. Concentrated hydrochloric acid (HCl, 35%), ammonia solution (NH_3, 35%) and toluene (HPLC grade) were all supplied by Fisher Scientific. 3-Amminopropyltriethoxysilane (APTES, 99%) was purchased from Fluorochem. Ethanol (99.5%) and sodium hypochlorite (12% aqueous solution) were supplied by Synth, Brazil. The tomatoes seeds (*Solanum Lycopersicum*) were purchased from ISLA Sementes, Porto Alegre, Rio Grande do Sul-Brazil.

2.2 Synthesis and functionalization of Fe_3O_4 magnetic nanoparticles (MNP)

2.2.1 Preparation of magnetic nanoparticles MNP

The co-precipitation method was used to prepare the MNP as published previously by Zhao et al. (2015).[16] Firstly, 5.4 g of iron (III) chloride hexahydrate was dissolved in 20 mL of deionized water and 2.0 g of iron (II) chloride was dissolved in 5 mL of a solution of 2 M hydrochloric acid. Both solutions were added to 100 mL of deionized water and mixed thoroughly in a round-bottom flask (250 mL) with mechanical stirring using an overhead stirrer (IKA). A 2 M solution (120 mL) of ammonia was then added to the reaction mixture slowly to precipitate Fe_3O_4 nanoparticles (MNPs). The reaction lasted for 10 minutes at room temperature and the speed of the overhead stirring was set at 300 rpm. The black MNPs in suspension were then transferred to a beaker (250 mL) and recovered using a neodymium iron boron (NdFeB) magnet. These MNPs were then washed using deionized water (100 mL) until the solution was neutral (pH 7); this usually takes approximately 10 washes. In order to avoid moisture, the particles were then suspended in toluene for further experiments.

2.2.2 Functionalization of MNP using APTES

Amine groups were grafted onto the MNP surface via silanization using 3-amminopropyltriethoxysilane (APTES) following a prior work.[17] Generally, 0.5 g of the prepared MNP was suspended in 100 mL of dry toluene in a round-bottom flask (250 mL). The suspension was then sonicated in an ultrasonic bath for 10-15 minutes until the magnetic nanoparticles were fully dispersed in toluene. Approximately a 1:1 mass ratio of APTES to MNP is used for the synthesis reaction as 0.5 mL of APTES was added to the suspension dropwisely. Excessive APTES was used to ensure complete coverage of the surface on MNPs.

The reaction mixture was then heated to a reflux using a hot oil bath at 110°C under mechanical stirring at 300 rpm for 6 h. Once this silanization reaction was completed, the sample, denoted as NH_2-MNP, was washed with acetone (20 mL) with sonication for at least 8 times to remove unreacted APTES and residual toluene. Acetone was finally removed using a vacuum oven (Heraeus) at 50°C for at least 8 h.

2.2.3 Polycaprolactone (PCL) coating onto NH_2-MNP

Polycaprolactone (PCL) was bound on to the NH_2-MNP particles via thermal coupling, based on a method published previously.[18] In brief, 100 mg of NH_2-MNP (from section 2.2.2) were suspended in 20 mL of dry toluene in a round bottom flask (250 mL) and sonicated at 70°C until full dispersion. PCL (2 g) was dissolved separately in 20 mL of dry toluene and heated to 70°C. This PCL-toluene solution was then added to the NH_2-MNP suspension dropwisely and the reaction mixture was then heated to 110°C under mechanical stirring (300 rpm) for at least 8 h. The resultant PCL-MNP was recovered using a NdFeB magnet and washed with acetone using an ultrasonic bath to remove unreacted polymer and solvent. Acetone was finally removed using a vacuum oven (Heraeus) at 50°C for at least 8 h.

2.3 Characterization of magnetic nanoparticles

Transmission Electron Microscopy (TEM) imaging was used to examine the materials on a nanoscale. The images were taken using a FEI TECNAI TF20 microscopy fitted with a field emission gun and operated at 200 keV. The sample (< 0.1 mg) was suspended in ethanol using sonication and then deposited on a holey carbon (300 mesh) sample grid (Agar). The prepared sample grid needed to be dried in air for at least 24 h before analysis.

The organic coating on magnetic nanoparticles was characterized using Fourier-transform infrared (FTIR) spectroscopy. The analysis was carried out using a Perkin Elmer Spectrum 100 spectrometer fitted with an ATR sampling unit. For sample measurements, 32 scans in the region from 650 to 4000 cm^{-1} were recorded with a resolution of 4 cm^{-1}. CHN elemental analysis was performed with an Exeter CE-440 Elemental Analyzer.

Thermogravimetric analysis (TGA) were carried out to quantify the organic content on MNP surface and performed using a TA instrument SDT Q600. Generally, the samples (*ca*. 5 mg) were heated up to 800 °C at a heating rate of 10°C/min, under air flow (100 mL/min).

The Dynamic light scattering (DLS) was used to study particle hydrodynamic diameter (nm) and polydispersity index (PDI). The measurements were performed using

a Zetasizer Nano ZS90 (Malvern Instrument, UK). The samples were dispersed in ultrapure water (0.1 mg/mL) and were measured in triplicate at 25°C with the scattered light detected at an angle of 90°C. The zeta potential values (mV) were determined by electrophoresis, with analysis in triplicate, at 25 °C, also using the Zetasizer ZS90 instrument (Malvern Instrument, UK).

2.4 Plant studies

2.4.1 Seed treatment

Tomato seeds (*Solanum Lycopersicum*) were sterilized in sequential washes for 1 min in 70% ethanol, 5 min in 2% sodium hypochlorite, and three times for 5 min in sterile deionized water. The seeds were treated with different concentrations of nanoparticles (0.25, 2.5 and 5 mg/mL). Typically, 50 seeds were added into a flask (which contained 10 ml of a given nanoparticle suspension) and then the flask was subjected to 24 hours of orbital shaking at 100 rpm in the dark at room temperature.[19]

2.4.2 Scanning Electron Microscopy (SEM) and Energy Dispersive X-ray (EDX) spectroscopy

Surface morphology and metal distribution of seed samples were studied by a scanning electron microscopy (SEM) and energy dispersive X-ray (EDX) spectroscopy. They were performed using Philips XL30 ESEM electron microscope with an Oxford Instruments X-act EDX detector. The EDX was calibrated using the INCA EDX software with Cu (99.999% purity) as the calibration standard. The SEM micrographs provided a visual representation of the morphology of the seed before and after MNP loadings while EDX mapping was used to study the localization of MNPs on the seed coats. Seeds were placed on carbon tape, followed by palladium sputtering to enhance the conductivity prior to imaging since the seed samples were insufficiently conductive. All micrographs and EDX spectra were recorded using a beam current of 20 kV.

2.4.3. Quantification of MNP loading on seeds using Atomic Absorption Spectroscopy (AAS)

Seeds loaded with MNP samples were digested in concentrated hydrochloric acid (1 mL), speeded up by sonication. The solution was then diluted with deionized water and the atomic adsorption intensity of solution was measured using a Thermo Fisher Flame Atomic Absorption Spectrometer (S series unit) fitted with an iron lamp (λ = 248.3 nm).

2.4.4. Seed analysis for Microprobe X-ray Fluorescence Spectroscopy (μ-XRF)

Tomato seeds were longitudinally cut using a razor blade, fixed in a proper sample holder sealed with a 6 μm thick polypropylene thin film (VHG, USA) and probed by a benchtop μ-XRF system (Orbis PC EDAX, USA). The samples were investigated along 64 points by a 30 μm X-ray beam generated by a Rh anode operating at 45 kV and 300 μA with a 25 μm Ti primary filter selected. The X-ray fluorescence photons were counted by silicon drift detector (SDD) and the dead time was smaller than 3%.[20] For each treatment, the iron intensities in the seed coat and endosperm regions were statistically compared by analysis of variance (ANOVA) with Tukey's post-hoc test ($p < 0.05$), using SAS 9.3 software.

Besides, tomato seeds were transversally mapped by the microprobe X-ray fluorescence. The elemental mapping images (Fe, Ca and K) were generated by a 32×25 pixel matrix investigated using the same instrumental conditions described above, but with a 500 μA current and 2 s of dwell time. The maps were obtained by interpolation using the OriginLab 2019. Figure S1 details the setup for the XRF analysis (S1-a) and the sample loaded into the equipment (S1-b).

2.4.5 Nanoparticles effects of tomato seedlings

To evaluate the effects of magnetic nanoparticles on plants, ten seeds were transferred to Petri plate (100 × 15 mm) containing solid agar (1.5%) for germination. The seeds were germinated in the dark for 5 days. The germination index, shoot and roots length (cm) and seedling dry weight (mg) data were then collected and statistically treated with calculation of the means and standard deviations (n=3 Petri plates with 10 seeds), followed by analysis of variance (ANOVA) with Tukey's post-hoc test ($p < 0.05$), using GraphPad Prism 5.01 software.

2.4.6. Seedling analysis by microprobe X-ray fluorescence spectroscopy (μ-XRF)

The distribution/localization of MNPs, coated and not coated with APTES and PCL, in tomato seedlings also were monitored by μ-XRF. Ten points distributed through the cotyledonary leaves, stem and radicle were investigated by a 30 μm X-ray beam generated by a Rh anode operating at 45 kV and 900 μA with a 25 μm Ti primary filter. The X-ray spectra were acquired using 30 s dwell time by a 30 mm^2 SDD detector. The dead time smaller than 10%. In this assay, seedlings obtained from seeds treated with 5 mg/mL of MNPs were used. The intensities recorded in the cotyledon leaves, stems and the radicle were statistically compared among the MNP treatments by analysis of variance (ANOVA) with Tukey's post-hoc test ($p < 0.05$), using SAS 9.3 software.

2.4.7. X-ray fluorescence spectroscopy data treatment

For all the XRF analysis, the instrumental limit of quantification (ILOQ) values were calculated. The values above the ILOQ were not considered in elemental maps (Fig. 4) of seeds and the probing of seedlings (Fig. 7), whereas it was denoted with a red dashed line in the linescans of seeds (Fig. 5). The ILOQ was calculated in according to the equation (1):

$$ILOQ=8.485\times(BGt)12 \quad (1)$$

where *BG* is the average of background count rate under the XRF analyte signal, and *t* (in s) is the dwell time.

Moreover, the XRF analysis, the Fe, Ca and K intensities were divided by the Rh Kα Compton scattering of the corresponding probed points, and subsequently, by their corresponding elemental sensitivities, determined throughout reading Fe, K, and Ca thin film standards (MicroMatter™, Fe: 49.4; K: 26.69, Ca: 30.90 μg cm^{-2}) at the same instrumental conditions employed for the samples, in according to the equation (2):

$$S=IC \quad (2)$$

where S is the elemental sensitivity (in μg^{-1} cm^2), I is the intensity of the thin film standard (a.u.), and C is the elemental concentration on the thin film (μg cm^2).

3. Results and Discussions

3.1 Nanoparticles characterization

Results from the characterization of MNP samples using TEM, DLS, electrophoresis (zeta potential), FTIR and TGA are shown in Figure 1. Figure 1a shows typical TEM images of unfunctionalized MNPs. The particle size was measured and the size distribution was shown in Figure 1b (n = 110). The majority (90%) of the particles are between 6-13 nm wide with mean diameter around 9 nm. The nanoparticles size found in this study is consistent with those reported in the literature.[11,21] The hydrodynamic diameter from DLS was 4 ± 0.5 nm with PDI of 0.29 ± 0.03. When functionalized with APTES (NH_2-MNPs), there was no observable change in size distribution. With PCL coating, the size of the nanoparticles increased to 76 ± 0.3 nm with PDI 0.25 ± 0.002. This is due to aggregation and crosslinking between particles.

The uncoated MNPs showed zeta potential of –6 ± 0.4 mV, which is near neutral. The surface functionalization via silanization consists in a condensation reaction between the hydroxyl groups from MNPs and siloxane groups from APTES.[21] The grafting of amines can be confirmed by an increase in zeta potential to a positive value, since the nanoparticle surface becomes positively charged in a neutral/acidic pH. Consequently, the NH_2-MNP showed zeta potential of +37 ± 0.4 mV. The PCL coating reduced the zeta potential slightly to +27 ± 2.9 mV, as some surface amine groups had reacted with PCL carboxylic acid groups during thermal coupling.

The identity of the surface functional groups on MNPs were examined using FTIR and the spectra are shown in Figure 1e. The additional bands indicate that the corresponding functional groups were coated on MNP surfaces. The FTIR spectrum of NH_2-MNP presented bands at 1000 cm^{-1}, attributed to the Si-O-Si groups. The bands at 1595 and 3440 cm^{-1} are due to the N-H stretching vibration and free NH_2 groups.[21] After coating with PCL, the PCL-MNP nanoparticles showed bands at 1730 cm^{-1} (C=O, stretch, ester), 1640 cm^{-1} (C=O, stretch, amide) and 1300 cm^{-1} (C-O-C, stretch asymmetric). These bands represent the ester structure in PCL.[22] The organic content on the MNP surface was quantified using TGA and (figure 1f). There is a weight gain of

1.4% observed from unfunctionalized-MNP at around 200°C due to the oxidation from Fe_3O_4 to Fe_2O_3, a consistent observation to published works.[17] The NH_2-MNP lost 3.5% weigh due to organic content while PCL-MNP lost *ca*. 8% weigh due to the polymer coating.

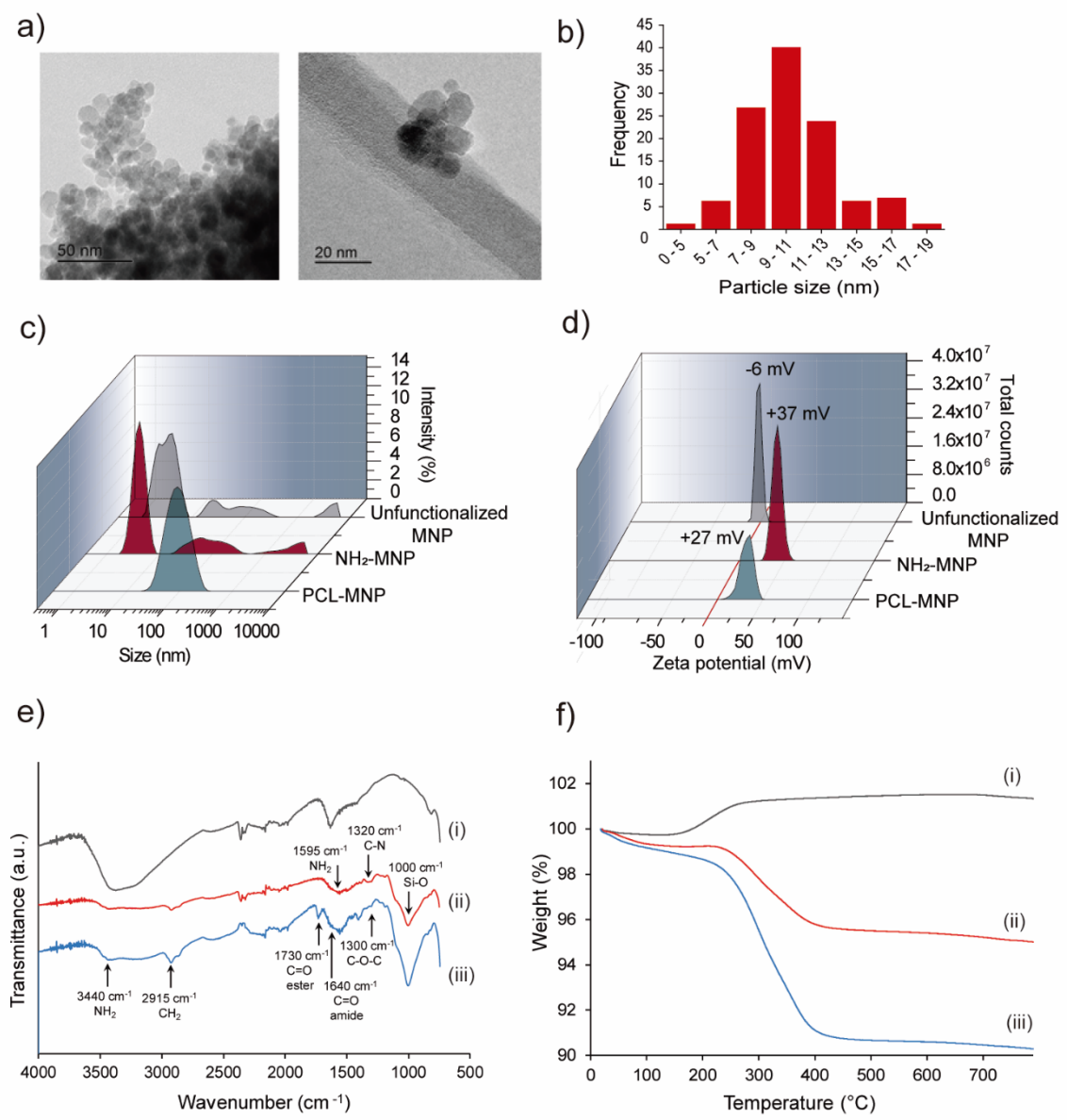

Figure 1: Nanoparticles characterization by (a) TEM images, (b) size distribution from TEM(n=110), (c) size distribution from DLS, (d) zeta potential, (e) FTIR spectra and (f) TGA curves for the unfunctionalized-MNP (i) NH_2-MNP (ii) and PCL-MNP (iii).

3.2 MNP nanoparticles localization on seed coats: SEM/EDX study

The adsorption of MNP on tomato seeds, kept in aqueous suspension, was evidenced by the change in their external color to brownish color and their response to an external magnetic field. As shown in Figure 2, the extent of adsorption promotes sufficient deposition of the three MNP to make the seeds magnetic.

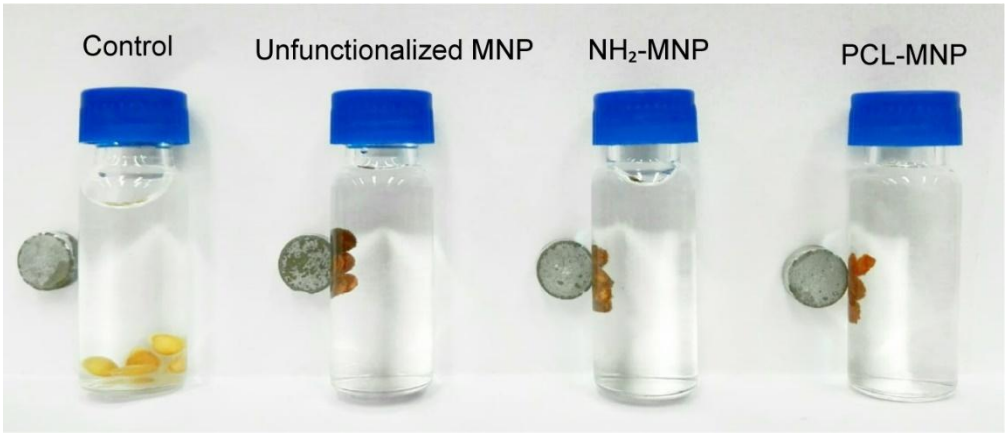

Figure 2. Tomato seeds treated for 12 hours in aqueous suspension of MNP samples.

SEM-EDX revealed seed morphology and MNPs localization. The top panel of SEM micrographs in Figure 3 shows that the morphology of seeds was not altered by the MNP loading. At a higher magnification, the MNPs were found trapped inside the fibers on the seed coat (middle panels). There is no observable difference between MNPs with different surface functionality. Localization of MNPs was highlighted by the EDX mapping (bottom panels) as strong iron (Fe) signals were recorded. Further analysis using EDX spectroscopy (Figure S2) on the seed surface confirmed the identity of the particles as there was no Fe signal from the control sample. A Fe signal was observed for all MNP-loaded seeds, while seeds loaded with NH_2-MNP and PCL-MNP nanoparticles also showed an enhanced carbon (C) signal due to the propylamine chain on APTES and PCL polymer. This result indicates that this MNP system can adapt to a wide range of surface functionalities, allowing further development as carriers for delivery of (bio)molecules including bio-active reagents, e.g. pesticides. There is also no observable damaging effect on seeds, suggesting that application of these MNP systems to plants are possible with minimal adverse effects. The amount of MNPs loading on seeds was also quantified using AAS (Figure S3). The results suggested that around 0.018 – 0.029 mg MNPs were loaded onto 1 mg of seed, equivalent to around 1.8 – 2.9%.

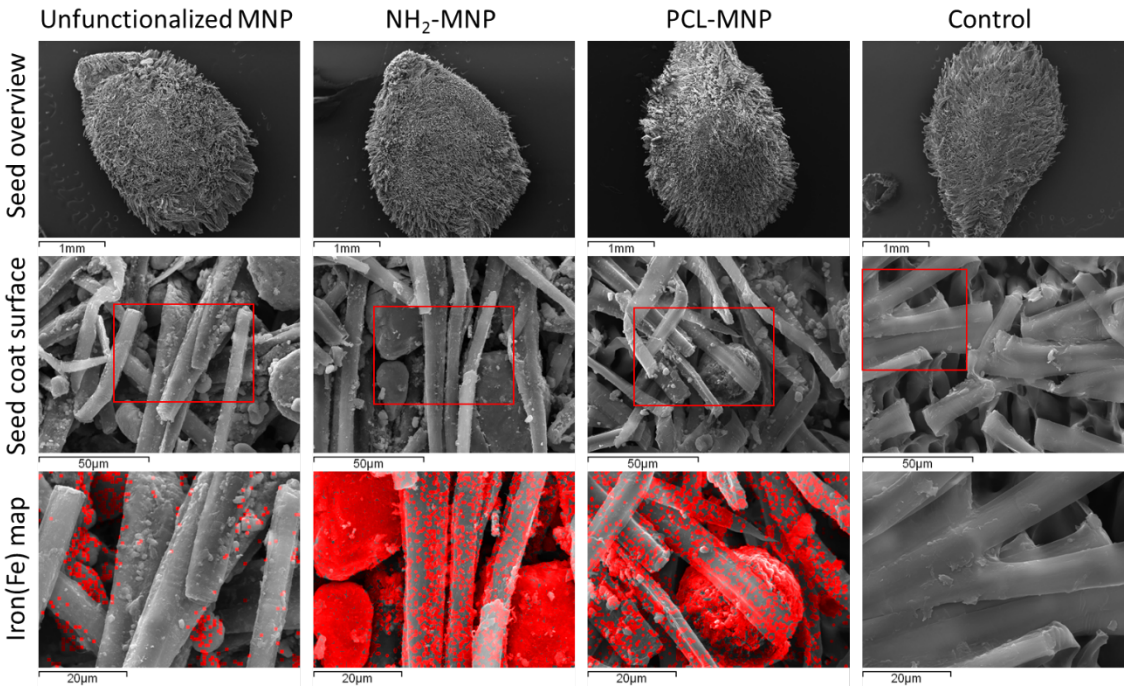

Figure 3: Scanning Electron Microscopic (SEM) images for seed samples loaded with MNP at 5 mg/mL. Images at the top panel show the overviews while in the middle panel, images with a higher magnification show the morphology of coats before and after MNP loadings. The iron maps from EDX are shown in the bottom panel, the areas of interests are indicated as red rectangles in the middle panel. No iron was detected in the control sample.

3.3 Nanoparticle uptake in seeds: X-ray fluorescence (XRF) evaluation

Further analysis for determining the distribution/localization of MNPs in seeds was carried out using XRF elemental mapping. Figure 4 shows microscopic images and the µ-XRF elemental maps for calcium (Ca), potassium (K) and iron (Fe) for *S. lycopersicum* seeds. The chemical maps reveal high intensity of the Ca at the seed coat region (second column, ii), while the K is found in the endosperm (third column, iii). In addition, hotspots of K intensity are observed in the embryo region. The counting rate of both Ca and K intensities, however, are very similar among the treatments and the control.

On the other hand, Fe intensity increased substantially in the treated seeds (Figure 4 b.iv, c.iv and d.iv). The line scan measurements (Figure 5) indicate that most MNPs remained in the seed coat, this is statistically confirmed for seeds treated with PCL-MNP and unfunctionalized-MNP (Figure S4a).

Statistical analysis in Figure S4c also show that the amount of iron in the endosperm of treated seeds was higher than that found for the control ones, following the sequence NH_2-MNP > PCL-MNP ≈ unfunctionalized-MNP > control. It is worth to note that, even though we performed several seed cuts and they were reproducible, one cannot exclude the possibility the part of iron observed in the endosperm have been dragged during sample slicing. However, the median number of counts at the endosperm of treated seeds were from three to ten-fold higher than that of control (control: 3.1×10^{-4}; NH_2-MNP: 3.3×10^{-3}; PCL-MNP: 1.1×10^{-3}; unfunctionalized MNP: 1.2×10^{-3}; unit: counts µg cm^2), thus, excluding the contribution of spikes from dragged MNP.

These results were consistent with literature results for bean seeds (*Phaseolus vulgaris* L.) soaked in a 5.0 mg mL^{-1} solution (similar concentration to our study) containing 25 and 40 nm CuO NPs and 20, 40, 60 nm ZnO NPs.[23] Among the three seed samples loaded with MNPs, no difference was observed in the distribution of Fe at the surface of the seeds. This observation suggests that the particle adsorption was not influenced by surface groups or surface chemistry of MNPs.

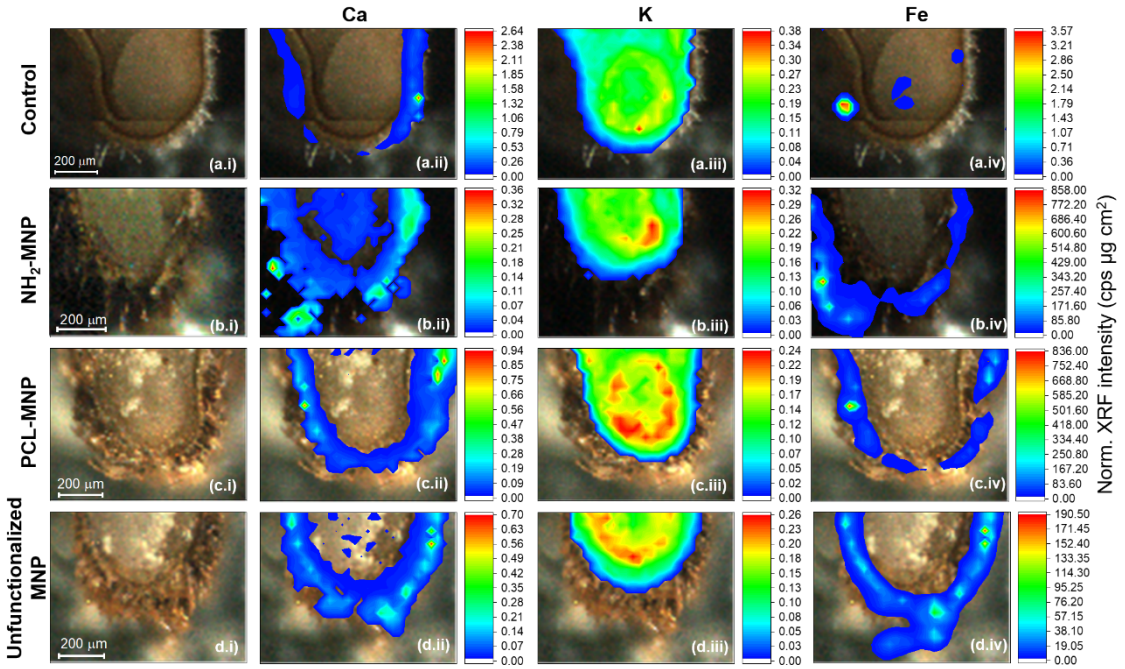

Figure 4: Seed images on left side (a.i, b.i, c.i and d.i) and X-ray fluorescence chemical revealing the spatial distribution of Ca (a.ii, b.ii, c.ii and d.ii), K (a.iii, b.iii, c.iii and d.iii) and Fe (a.iv, b.iv, c.iv and d.iv) of tomatoes (*Solanum lycopersicum*) treated with various MNP samples at 5 mg/mL.

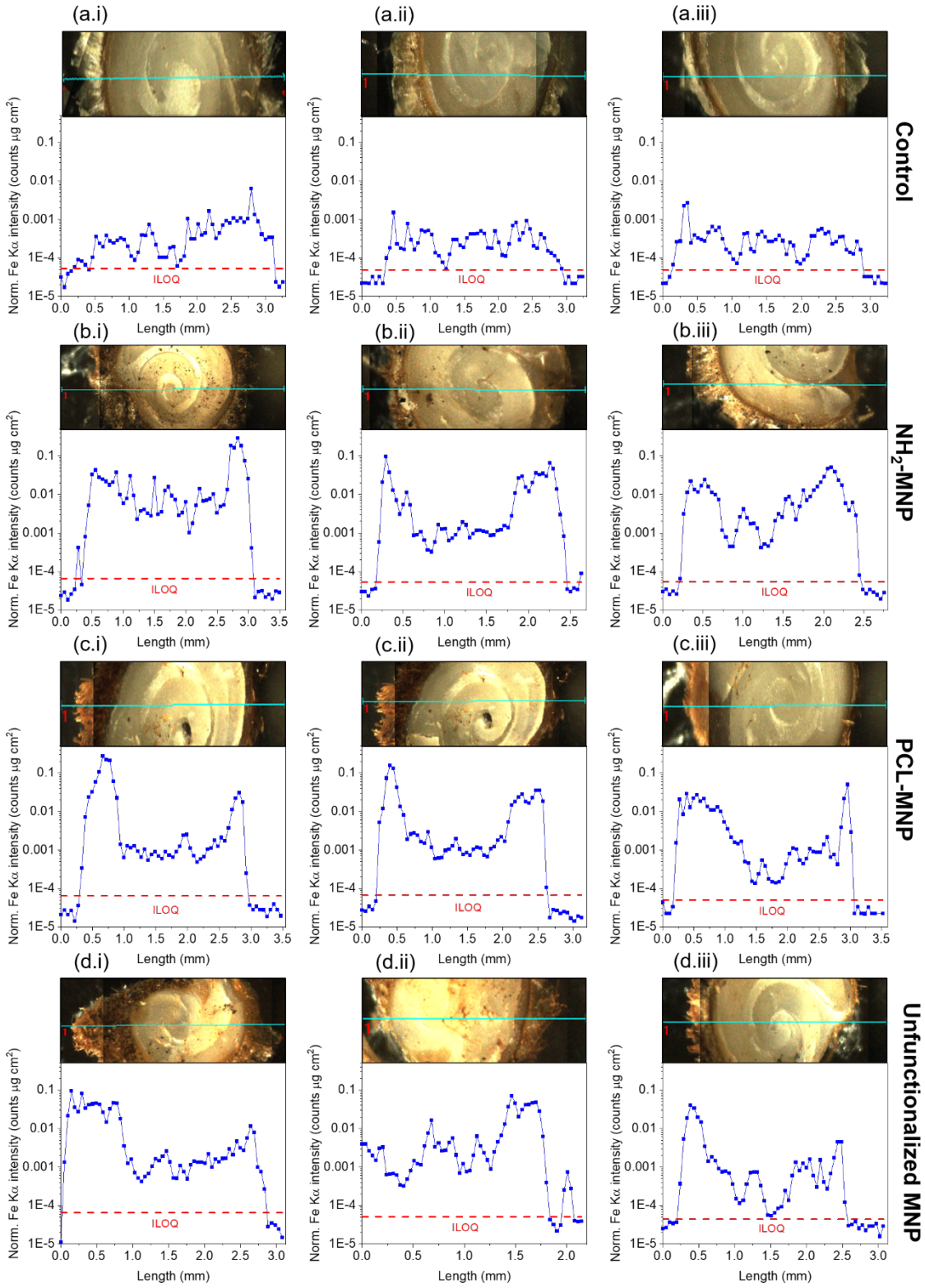

Figure 5. XRF longitudinal line scans for tomato seeds. The dashed red line refers to the instrumental limit of quantification (ILOQ) for Fe. Samples are represented by (a) control, (b) NH_2-MNP, (c) PCL-MNP and (d) Unfunctionalized-MNP. In all seeds

treated with Fe sources, the number of Fe counts was higher on the seed surface and on the hilum region. All measurements were made in triplicate (i, ii, iii).

3.4 Biological evaluation in tomatoes seeds

Following seed priming, the seeds were sown in Petri dishes, and then 5 days later evaluated in relation to the shoot and root size, and dry mass of the plant (Figure 6). For all treatments the germination index was 100% (data not shown), and the treatment with three MNP samples did not promote observable effects on root size, shoot size and dry mass compared the control. It indicates that the nanoparticles evaluated in this study did not affect plant growths in the initial stage. Therefore, the MNPs might be applied to plants without detectable side effects. This is consistent with relevant research works in the literature where iron oxide nanoparticles were found to be non-toxic to the plants, and could even stimulate plant development.[11,14,15]

According Sundaria and co-workers (2019), the effects of 80 nm γ-Fe_2O_3 (maghemite) nanoparticles for wheat seed priming were dependent on the nanoparticle concentration.[13] Concentration at 0.6 mg/mL inhibited seed germination, while concentrations below 0.2 mg/mL can stimulate the germination as well as increase the nanoparticles uptake by the seeds. Reactive oxygen intermediates formed during seed germination may increase the germination percentage, but in large amounts, the presence of transition metals leads to excessive formation of hydroxyl radicals via the Fenton reaction and may cause damage to plant DNA.[13,24] Another study by Duran et al. (2018) also showed that Fe_3O_4 nanoparticles (*ca*. 12-14 nm at 1 to 1000 mg Fe/L or 1.38 x 10^{-3} to 1.38 mg/mL) stimulated the radicle growth of *Phaseolus vulgaris* seedlings (8.1 ± 1.1 cm *vs*. 5.9 ± 1.0 cm for the control). A key factor that triggered the observed results was the poly(ethylene glycol) (or PEG) coating on nanoparticle, inducing an increase in water uptake.[25] In the present work, there was no growth inhibition observed up to 5 mg/mL of these MNP samples.

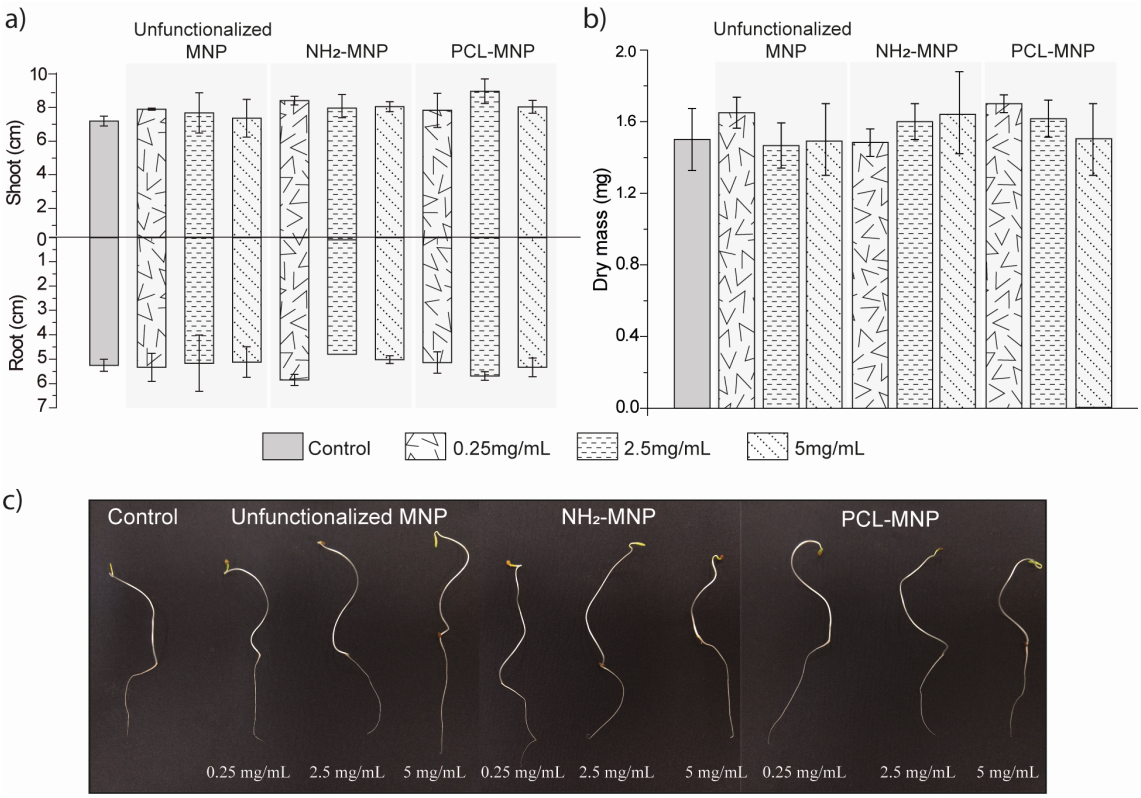

Figure 6: Evaluation of seedlings sprout from seeds treated with magnetic nanoparticles. The figure corresponds to root and shoot length data (a), dry mass of the plant (b), and image of seedlings after 5 days of seeding (c). The results represent the average of 3 Petri plates, containing a total of 10 seeds per plate. Statistical analyses were performed using one-way ANOVA with Tukey's test and none of the comparisons were significant (significance level of $p < 0.05$).

3.5 Nanoparticle uptake in tomato seedlings: A microprobe X-ray fluorescence (μ-XRF) evaluation

Localization of MNPs post germination would be of particular interest if this MNP system is to be developed for the delivery of bio-active agents. Figure 7 shows the iron distribution in different parts of tomato seedlings loaded with MNP samples. Higher XRF counts for iron in seedlings germinated from treated seeds showed that iron was transferred from seed to root and cotyledon during the germination process. Comparing the iron count in the different parts of the seedlings with the control, it is observed that the uptake by seedlings occurs more expressively for unfunctionalized MNPs, while both functionalized MNPs showed similar iron count distribution to the control. Since NH_2-MNPs and PCL-MNPs have similar zeta potential while the unfunctionalized MNPs and NH_2-MNPs have similar hydrodynamic size, surface

charge could be the predominant factor over particle size in influencing the translocation of particles in seedlings.

However, results in reported literature are not always coherent and factors influencing uptake can be complex. First is the size of nanoparticles. Generally, small nanoparticles are more likely to be taken up by the seeds than larger nanoparticles.[26] In our study, the hydrodynamic size of NH_2-MNPs is 4 ± 0.5 nm while MNPs coated with PCL increase to 76 ± 0.3 nm in size but showed no difference in translocation Instead, our results showed that the charge of nanoparticle surface could override the size factor as NH_2-MNPs have comparable hydrodynamic size as unfunctionalized MNPs. Studies in the literature have also shown that surface charge (or zeta potential) can influence the nanoparticle uptake in plants where nanoparticles with a positive zeta potential are retained in the seeds coated due to the interactions with proteins. On the other hand, negatively charged nanoparticles are more likely to cross the seed coating.[27-29] Systematic studies on the particle parameters including size, charge, surface functionality and even shape are needed to fully understand the relationship between particle uptake, interaction with plants and their translocation.

Hence, the functionalization and coating appear to provide a barrier to internalization and uptake of the MNPs into tomato seedlings. Although unfunctionalized MNPs showed a better uptake they are unlikely to act as carriers of bio-active reagents. From this perspective, since both PCL-MNPs and NH_2-MNPs still showed preferential localization towards the cotyledons and root they can be of particular interest for food production and disease treatments. Since the phytotoxicity tests showed that these nanoparticles did not affect plant development in relation to germination and plant growth, both NH_2-MNP and PCL-MNP have shown promising potential for agricultural applications. For example, they can act as viable nanocarrier systems for the targeted pesticides delivery systems that could be more effective and less harmful to the environment. In particular, they can be suitable as vehicles for specific delivery of pesticides, and among other desired reagents, to the cotyledons or roots. Nevertheless, more research on their effects in other plants and organism models using different techniques is required to guarantee their safe application. Moreover, since plant species react to nanoparticles in various ways, evaluation of factors such as the production of reactive oxygen species (ROS), changes in gene regulation and changes in nutrient content, and among other factors, is necessary for understanding the safety effect of MNPs.

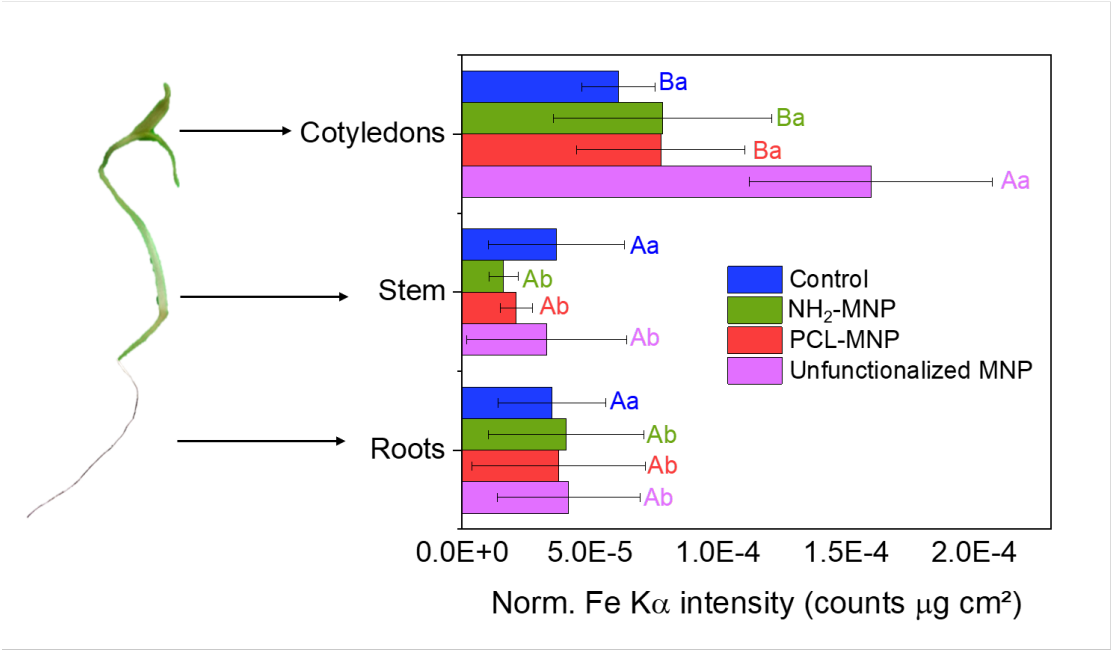

Figure 7. XRF iron counts at cotyledon leaves, stem and root of tomato seedlings exposed to MNPs. The counts represent the average of the measurements in three independent measurements (n = 3). Statistical analyses were performed using one-way ANOVA with Tukey's test and none of the comparisons (significance level of $p < 0.05$). The capital letters compare the effect of different treatments within a specific tissue. Lower case letters compare the effect of a single treatment on the different tissues.

4. Conclusions

In conclusion, the surface of Fe_3O_4 MNPs with the average size of 9 nm can be functionalized with amine-groups and polycaprolactone. No appreciable size increases were observed for amine-functionalized NP while after the coating with (PCL) their average size increased to 76 nm. These MNPs can be internalized into the seeds. Although the XRF mappings and line scans showed a variation in iron content across the seeds; the internalization of the seeds was mostly located in the seed coating. XRF also showed that the functionalization and coating of MNPs considerably reduced the presence of iron in the cotyledon that hinders nanoparticle uptake and translocation. The reason for the preferential translocation of nanoparticle is still unclear and further

studies are required to fully understand the phenomenon. However, the phytotoxicity tests showed that these nanoparticles did not affect plant development in relation to germination and plant growth. The phytotoxicity tests show that these nanoparticles have no detrimental effect on plant development in relation to germination and plant growth. Therefore, both NH_2-MNP and PCL-MNP could be promising targets for agricultural applications. For example, they can act as viable nanocarrier systems for the targeted pesticides delivery systems that could be more effective for stimulating plant growth and less harmful to the environment. Nevertheless, still, it is necessary to investigate the effects in other plants and organisms' models using different techniques to guarantee its safe application. Besides, as plants react to NPs in various ways, the evaluation of factors such as the production of reactive oxygen species, changes in gene regulation and changes in nutrient content, among other factors, is necessary for understanding fully the safety of MNPs.

Furthermore, the ability of polycaprolactone coated nanoparticles to deliver atrazine herbicide was previously demonstrated.[30] The produced formulation remained stable and showed good herbicidal activity at relatively low concentrations compared to commercial formulations. Thus, the PCL-MNP samples prepared in this study could serve as a platform for further development of asset delivery systems. Moreover, since they are externally aggregated to seeds, these MNPs can be used as carriers for seed treatment for seed priming to deliver nutrients in the early stage of plant development or seed coating for pest control**.**

6. Acknowledgments

The authors are grateful to São Paulo Research Foundation (FAPESP grants 2015/05942-0, 2015/19121-8, 2017/21004-5 and 2018/23608-8). Also, HHPY would like to thank FAPESP-CONFAP-Newton Fund for the visiting research grant (2018/02413-4). The authors acknowledge financial support from the Engineering and Physical Sciences Research Council EPSRC grant number EP/L016419/1 for Ph.D. studentship to ECHTL via the CRITICAT program. The scholarships of GSM and CGC are sponsored by Agrichem and Agrivalle, respectively.

7. Supplementary Information. Figure S1. Setup for µ-XRF analysis. Figure S2. EDX spectra of MNP-loaded seeds. Figure S3. Quantification of Fe_3O_4 MNP on seeds using AAS. Figure S4. Statistical analysis on the µ-XRF data on seed coats and endosperm.

8. References

(1) Kah, M.; Beulke, S.; Tiede, K.; Hofmann, T. Nanopesticides: State of Knowledge, Environmental Fate, and Exposure Modeling. *Critical Reviews in Environmental Science and Technology* **2013**, *43* (16), 1823–1867. https://doi.org/10.1080/10643389.2012.671750.

(2) Prajitha, N.; Athira, S. S.; Mohanan, P. v. Bio-Interactions and Risks of Engineered Nanoparticles. *Environmental Research*. Academic Press Inc. May 1, 2019, pp 98–108. https://doi.org/10.1016/j.envres.2019.02.003.

(3) Pérez-de-Luque, A. Interaction of Nanomaterials with Plants: What Do We Need for Real Applications in Agriculture? *Frontiers in Environmental Science* **2017**, *5*. https://doi.org/10.3389/fenvs.2017.00012.

(4) Nel, A.; Xia, T.; Mädler, L.; Li, N. Toxic Potential of Materials at the Nanolevel. *Science*. February 3, 2006, pp 622–627. https://doi.org/10.1126/science.1114397.

(5) Tombuloglu, H.; Slimani, Y.; Tombuloglu, G.; Almessiere, M.; Baykal, A. Uptake and Translocation of Magnetite (Fe3O4) Nanoparticles and Its Impact on Photosynthetic Genes in Barley (Hordeum Vulgare L.). *Chemosphere* **2019**, *226*, 110–122. https://doi.org/10.1016/j.chemosphere.2019.03.075.

(6) Siddiqi, K. S.; Husen, A. Engineered Gold Nanoparticles and Plant Adaptation Potential. *Nanoscale Research Letters*. Springer New York LLC December 1, 2016. https://doi.org/10.1186/s11671-016-1607-2.

(7) Rizwan, M.; Ali, S.; Qayyum, M. F.; Ok, Y. S.; Adrees, M.; Ibrahim, M.; Zia-ur-Rehman, M.; Farid, M.; Abbas, F. Effect of Metal and Metal Oxide Nanoparticles on Growth and Physiology of Globally Important Food Crops: A Critical Review. *Journal of Hazardous Materials* **2017**, *322*, 2–16. https://doi.org/10.1016/j.jhazmat.2016.05.061.

(8) Avellan, A.; Yun, J.; Zhang, Y. L.; Spielman-Sun, E.; Unrine, J. M.; Thieme, J.; Li, J. R.; Lombi, E.; Bland, G.; Lowry, G. V. Nanoparticle Size and Coating Chemistry Control Foliar Uptake Pathways, Translocation, and Leaf-to-Rhizosphere Transport in Wheat. *ACS Nano* **2019**, *13* (5), 5291–5305. https://doi.org/10.1021/acsnano.8b09781.

(9) Avellan, A.; Schwab, F.; Masion, A.; Chaurand, P.; Borschneck, D.; Vidal, V.; Rose, J.; Santaella, C.; Levard, C. Nanoparticle Uptake in Plants: Gold Nanomaterial Localized in Roots of *Arabidopsis Thaliana* by X-Ray Computed Nanotomography and Hyperspectral Imaging. *Environmental Science & Technology* **2017**, *51* (15), 8682–8691. https://doi.org/10.1021/acs.est.7b01133.

(10) Kumar, V.; Guleria, P.; Kumar, V.; Yadav, S. K. Gold Nanoparticle Exposure Induces Growth and Yield Enhancement in Arabidopsis Thaliana. *Science of the Total Environment* **2013**, *461–462*, 462–468. https://doi.org/10.1016/j.scitotenv.2013.05.018.

(11) Rui, M. M; Ma, C. X.; Hao, Y.; Guo, J.; Rui, Y. K.; Tang, X. L.; Zhao, Q.; Fan, X.; Zhang, Z. T.; Hou, T. Q.; Zhu, S. Y. Iron Oxide Nanoparticles as a Potential Iron Fertilizer for Peanut (Arachis Hypogaea). *Frontiers in Plant Science* **2016**, *7*. https://doi.org/10.3389/fpls.2016.00815.

(12) Hussain, A.; Ali, S.; Rizwan, M.; Rehman, M. Z. U.; Qayyum, M. F.; Wang, H. L.; Rinklebe, J. Responses of Wheat (Triticum Aestivum) Plants Grown in a Cd Contaminated Soil to the Application of Iron Oxide Nanoparticles. *Ecotoxicology and Environmental Safety* **2019**, *173*, 156–164. https://doi.org/10.1016/j.ecoenv.2019.01.118.

(13) Sundaria, N.; Singh, M.; Upreti, P.; Chauhan, R. P.; Jaiswal, J. P.; Kumar, A. Seed Priming with Iron Oxide Nanoparticles Triggers Iron Acquisition and Biofortification in Wheat (Triticum Aestivum L.) Grains. *Journal of Plant Growth Regulation* **2019**, *38* (1), 122–131. https://doi.org/10.1007/s00344-018-9818-7.

(14) Li, J. L.; Chang, P. R.; Huang, J.; Wang, Y. Q.; Yuan, H.; Ren, H. X. Physiological Effects of Magnetic Iron Oxide Nanoparticles towards Watermelon. *Journal of Nanoscience and Nanotechnology* **2013**, *13* (8), 5561–5567. https://doi.org/10.1166/jnn.2013.7533.

(15) Kasote, D. M.; Lee, J. H. J.; Jayaprakasha, G. K.; Patil, B. S. Seed Priming with Iron Oxide Nanoparticles Modulate Antioxidant Potential and Defense-Linked Hormones in Watermelon Seedlings. *ACS Sustainable Chemistry & Engineering* **2019**, *7* (5), 5142–5151. https://doi.org/10.1021/acssuschemeng.8b06013.

(16) Zhao, H. Y.; Liu, S.; He, J.; Pan, C. C.; Li, H.; Zhou, Z. Y.; Ding, Y.; Huo, D.; Hu, Y. Synthesis and Application of Strawberry-like Fe_3O_4-Au Nanoparticles as CT-MR Dual-Modality Contrast Agents in Accurate Detection of the Progressive Liver Disease. *Biomaterials* **2015**, *51*, 194–207. https://doi.org/10.1016/j.biomaterials.2015.02.019.

(17) Yiu, H. H. P.; Bouffier, L.; Boldrin, P.; Long, J.; Claridge, J. B.; Rosseinsky, M. J. Comprehensive Study of DNA Binding on Iron(II,III) Oxide Nanoparticles with a Positively Charged Polyamine Three-Dimensional Coating. *Langmuir* **2013**, *29* (36), 11354–11365. https://doi.org/10.1021/la400848r.

(18) Nhavene, E.; Andrade, G.; Faria, J.; Gomes, D.; Sousa, E. Biodegradable Polymers Grafted onto Multifunctional Mesoporous Silica Nanoparticles for Gene Delivery. *ChemEngineering* **2018**, *2* (2), 24. https://doi.org/10.3390/chemengineering2020024.

(19) Pereira, A. do E. S.; Oliveira, H. C.; Fraceto, L. F. Polymeric Nanoparticles as an Alternative for Application of Gibberellic Acid in Sustainable Agriculture: A Field Study. *Scientific Reports* **2019**, *9* (1). https://doi.org/10.1038/s41598-019-43494-y.

(20) Rodrigues, E. S.; Gomes, M. H. F.; Duran, N. M.; Cassanji, J. G. B.; da Cruz, T. N. M.; Sant'Anna Neto, A.; Savassa, S. M.; de Almeida, E.; Carvalho, H. W. P. Laboratory Microprobe X-Ray Fluorescence in Plant Science: Emerging Applications and Case Studies. *Frontiers in Plant Science* **2018**, *871*. https://doi.org/10.3389/fpls.2018.01588.

(21) Wang, G. S.; Ma, Y. Y.; Tong, Y.; Dong, X. F. Synthesis, Characterization and Magnetorheological Study of 3-Aminopropyltriethoxysilane-Modified Fe_3O_4 Nanoparticles. *Smart Materials and Structures* **2016**, *25* (3). https://doi.org/10.1088/0964-1726/25/3/035028.

(22) Hivechi, A.; Bahrami, S. H.; Siegel, R. A. Drug Release and Biodegradability of Electrospun Cellulose Nanocrystal Reinforced Polycaprolactone. *Materials Science and Engineering C* **2019**, *94*, 929–937. https://doi.org/10.1016/j.msec.2018.10.037.

(23) Duran, N. M.; Savassa, S. M.; Lima, R. G. de; de Almeida, E.; Linhares, F. S.; van Gestel, C. A. M.; Pereira de Carvalho, H. W. X-Ray Spectroscopy

Uncovering the Effects of Cu Based Nanoparticle Concentration and Structure on *Phaseolus Vulgaris* Germination and Seedling Development. *Journal of Agricultural and Food Chemistry* **2017**, *65* (36), 7874–7884. https://doi.org/10.1021/acs.jafc.7b03014.

(24) Aruoma, O. I.; Halliwell, B.; Gajewski, E.; Dizdaroglu, M. Copper-Ion-Dependent Damage to the Bases in DNA in the Presence of Hydrogen Peroxide. *Biochemical Journal* **1991**, *273* (3), 601–604. https://doi.org/10.1042/bj2730601.

(25) Duran, N. M.; Medina-Llamas, M.; Cassanji, J. G. B.; de Lima, R. G.; de Almeida, E.; Macedo, W. R.; Mattia, D.; Pereira de Carvalho, H. W. Bean Seedling Growth Enhancement Using Magnetite Nanoparticles. *Journal of Agricultural and Food Chemistry* **2018**, *66* (23), 5746–5755. https://doi.org/10.1021/acs.jafc.8b00557.

(26) Wojcieszek, J.; Jiménez-Lamana, J.; Bierła, K.; Ruzik, L.; Asztemborska, M.; Jarosz, M.; Szpunar, J. Uptake, Translocation, Size Characterization and Localization of Cerium Oxide Nanoparticles in Radish (Raphanus Sativus L.). *Science of the Total Environment* **2019**, *683*, 284–292. https://doi.org/10.1016/j.scitotenv.2019.05.265.

(27) Bombo, A. B.; Pereira, A. E. S.; Lusa, M. G.; de Medeiros Oliveira, E.; de Oliveira, J. L.; Campos, E. V. R.; de Jesus, M. B.; Oliveira, H. C.; Fraceto, L. F.; Mayer, J. L. S. A Mechanistic View of Interactions of a Nanoherbicide with Target Organism. *Journal of Agricultural and Food Chemistry* **2019**, *67* (16), 4453–4462. https://doi.org/10.1021/acs.jafc.9b00806.

(28) Nguyen, M. H.; Lee, J. S.; Hwang, I. C.; Park, H. J. Evaluation of Penetration of Nanocarriers into Red Pepper Leaf Using Confocal Laser Scanning Microscopy. *Crop Protection* **2014**, *66*, 61–66. https://doi.org/10.1016/j.cropro.2014.08.016.

(29) Zhu, Z. J.; Wang, H. H.; Yan, B.; Zheng, H.; Jiang, Y.; Miranda, O. R.; Rotello, V. M.; Xing, B. S.; Vachet, R. W. Effect of Surface Charge on the Uptake and Distribution of Gold Nanoparticles in Four Plant Species. *Environmental Science and Technology* **2012**, *46* (22), 12391–12398. https://doi.org/10.1021/es301977w.

(30) Oliveira, H. C.; Stolf-Moreira, R.; Martinez, C. B. R.; Grillo, R.; de Jesus, M. B.; Fraceto, L. F. Nanoencapsulation Enhances the Post-Emergence Herbicidal Activity of Atrazine against Mustard Plants. *PLOS ONE* **2015**, *10* (7), e0132971. https://doi.org/10.1371/journal.pone.0132971.

TOC Graphic